

# Time-varying drainage basin development and erosion on volcanic edifices

Daniel O'Hara<sup>1,2</sup>, Liran Goren<sup>3</sup>, Roos M.J. van Wees<sup>1</sup>, Benjamin Campforts<sup>4</sup>, Pablo Grosse<sup>5,6</sup>, Pierre Lahitte<sup>7</sup>, Gabor Kereszturi<sup>8</sup>, Matthieu Kervyn<sup>1</sup>

<sup>1</sup>Department of Geography, Vrije Universiteit Brussel, Pleinlaan 2, 1050 Elsene.

<sup>2</sup>Helmholz Center Potsdam, GFZ German Research Center for Geosciences, Potsdam, Germany.

<sup>3</sup>Ben Gurion University of the Negev, Department of Earth and Environmental Sciences, Beer-Sheva, Israel

<sup>4</sup>Institute of Arctic and Alpine Research, University of Colorado Boulder, Boulder, CO, USA

<sup>5</sup>Consejo Nacional de Investigaciones Científicas y Técnicas (CONICET), Argentina

<sup>6</sup>Fundación Miguel Lillo, Miguel Lillo 251, (4000) Tucumán, Argentina

<sup>7</sup>Université Paris-Saclay, CNRS, Laboratoire GEOPS, Rue du Belvédère, 91405 Orsay, France

<sup>8</sup>Volcanic Risk Solutions, School of Agriculture and Environment, Massey University, 4474, New Zealand

*Correspondence to:* Daniel O'Hara (Daniel.OHara@vub.be)

**Abstract.** The erosional state of a landscape is often assessed through a series of metrics that quantify the morphology of drainage basins and divides. Such metrics have been well-explored in tectonically-active environments to evaluate the role of different processes in sculpting topography, yet relatively few works have applied these analyses to radial landforms such as volcanoes. We quantify drainage basin geometries on volcanic edifices of varying ages using common metrics (e.g., Hack's Law, drainage density, number of basins that reach the edifice summit, as well as basin hypsometry integral, length, width, relief, and average topographic slope). Relating these measurements to the log-mean age of activity for each edifice, we find that drainage density, basin hypsometry, basin length, and basin width quantify the degree of erosional maturity for these landforms. We also explore edifice drainage basin growth and competition by conducting a divide mobility analysis on the volcanoes, finding that young volcanoes are characterized by nearly-uniform fluvial basins within unstable configurations that are more prone to divide migration. As basins on young volcanoes erode, they become less uniform but adapt to a more stable configuration with less divide migration. Finally, we analyze basin spatial geometries and outlet spacing on edifices, discovering an evolution in radial basin configurations that differ from typical linear mountain ranges. From these, we present a novel conceptual model for edifice degradation that allows new interpretations of composite volcano histories and provides predictive quantities for edifice morphologic evolution.

## 1.0 Introduction

Understanding how drainage basins on eroding landforms develop and evolve is a fundamental principle of Geomorphology. Over regional scales, basin geometry, structure, and spacing evolve in response to both external (e.g., climate, tectonics; Castelltort et al., 2012; Duvall and Tucker, 2015; Han et al., 2015; Yang et al., 2015) and internal (e.g., channel piracy; Bishop, 1995; Whipple et al., 2016) forcing as topographic slopes adjust to develop and maintain an equilibrium between erosion and uplift (e.g., Willett et al., 2001; Castelltort et al., 2009). As these landscapes adjust, transient signals within basins propagate upstream to surrounding channel heads, where opposing signals between adjacent basins drive divide migration that modify available area for overland flow (e.g., Willett et al., 2014; O'Hara et al., 2019).

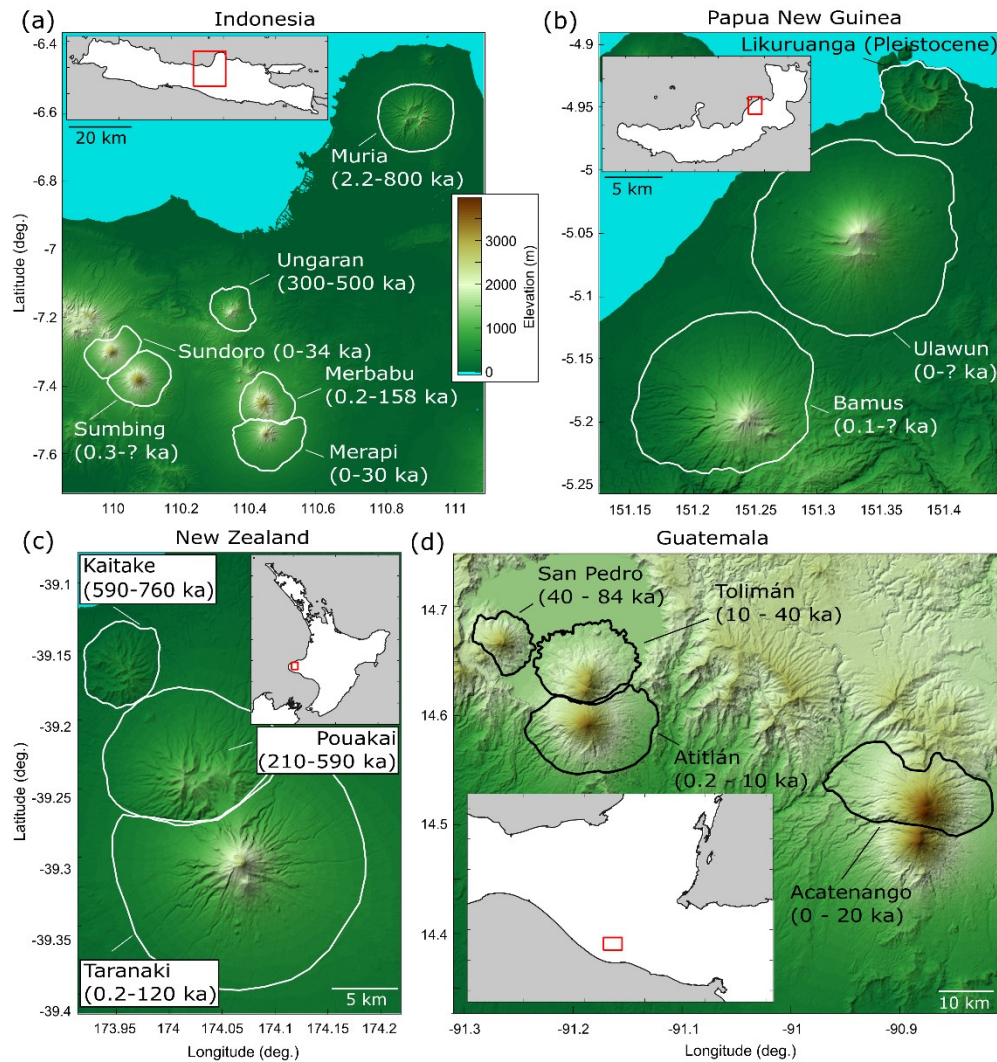
Work in the 20<sup>th</sup> century established foundational relationships between basin drainage areas, lengths, and slopes (e.g., Horton, 1945; Strahler, 1952; Hack, 1957; Flint, 1974), providing the basis for analyzing landscape disequilibrium and evolution in both tectonically-active (e.g., Kirby and Whipple, 2012; Fox et al., 2014) and passive (Prince and Spotila, 2013; Willett et al., 2014; Braun, 2018) regions. These relationships are built on the

42 assumption of a dominantly-dendritic fluvial network existing on a near-linear primary landform (e.g., a mountain  
43 range; Castelltort and Simpson, 2006). Furthermore, basin competition is often considered in the simplified  
44 configuration of a binary drainage system, where a divide supports only two opposing basins that compete across it  
45 (e.g., Gilbert, 1909; Mudd and Furbish, 2007).

46 Although dendritic channel networks are most prevalent on Earth, they are not the only type of configuration.  
47 Trellis, rectangular, parallel, and radial drainages also occur (Howard, 1967). The formation of these other drainages  
48 often relate to the region's tectonic, volcanic, or glacial history, subsurface structure, or geometry of the primary  
49 landform that they erode (Zernitz, 1932). However, compared to dendritic basins, studies that explore the geometries  
50 and evolution of other drainage settings are scarce (e.g., Mejía and Niemann, 2008; Becerril et al., 2021; Hamawi et  
51 al., 2022).

52 Volcanic edifices are characterized by radial drainages. In these settings, quantifying drainage evolution can be  
53 challenging as these landforms experience interspersed, short-term eruptive episodes superimposed onto the long-  
54 term degradation record (e.g., Thouret et al., 2014). These stochastic volcanic events often produce spatially-varying  
55 excess sediment supply in the form of pyroclasts with varying grain properties that significantly alter fluvial  
56 transport on decadal scales (e.g., Major et al., 2018; Hayes et al., 2002). Additionally, drainage formation can lag  
57 behind surfacing by volcanic deposits over 1 – 100 kyr timescales due to transmission losses associated with  
58 permeable volcanic material (e.g., lava flows, pyroclasts; Lohse and Dietrich, 2005; Jefferson et al., 2010; Sweeney  
59 and Roering, 2017). Finally, the more symmetric drainage divide configuration typical of linear mountain ranges  
60 breaks down on volcanic edifices due to their radial nature, with multiple catchments constrained to the conical  
61 structure of the volcano and converging towards one or a few main summits. Despite these challenges, volcanic  
62 edifices represent ideal primary landforms to investigate drainage evolution due to their well-defined conical initial  
63 conditions, datable surfaces, and scarce inheritance from regional tectonics. Furthermore, quantifying the  
64 relationships between edifice construction and drainage basin morphology provides new insight for investigating  
65 edifices remotely, and can thus expand our understanding of basin dynamics while also complementing field-based  
66 surveys to resolve volcano edifice histories.

67 Here, we explore the development of drainage basins and topography on stratovolcanoes from Indonesia, Papua  
68 New Guinea, New Zealand, and Guatemala (Fig. 1). Using common hydrographic metrics and broad volcanic  
69 histories, we determine stages of maturation during basin evolution and derive a new generalized model for  
70 stratovolcano degradation that builds off of previous studies (Ollier, 1988). We then quantify divide mobility on  
71 radial structures within the context of our conceptual model and discuss the applicability of our analyses to  
72 characterize an edifice's history.



73

74 **Figure 1** – Regional hillshaded relief maps of 16 analyzed edifices from (a) Indonesia, (b) Papua New Guinea, (c) New Zealand,  
 75 and (d) Guatemala. Maps are projected to 30 m UTM and use the same color scale. Solid white lines in a-c and solid black lines  
 76 in d represent edifice boundaries (boundary definition described in Methods). Text describes volcano names and known ages of  
 77 activity (Table T2). Insets are larger-scale regional maps for reference; gray areas represent ocean, white areas are land, and red  
 78 squares are bounds of hillshaded maps.

79 **2.0 Methods**

80 To constrain the temporal evolution of stratovolcano morphologies, we focus on closely-spaced volcano sets (Fig.  
 81 1). The advantages of this approach are that within each respective region, 1) volcanoes were likely fed by similar  
 82 magma sources (e.g., Locke and Cassidy, 1997; Haapala et al., 2005; Mulyaningsih and Shaban, 2020), constructed  
 83 by similar volcanic deposits, and thus had similar volcanic shapes, 2) edifices experienced similar climate  
 84 conditions, 3) volcano sets have radiometric ages related to their initiation and most recent eruption that are  
 85 comparable, providing constraints on their overall lifespan, and 4) volcanoes within the same set were active over  
 86 different time intervals, thus showing contrasting time-dependent degrees of dismantling within a short (10's of km)  
 87 distance. In order to consider drainage basin evolution through fluvial erosion from the perspective of radial  
 88 landforms, we exclude volcano massifs from our analysis, as well as any volcano with recognizable collapse scars,

89 and only consider volcanoes that do not have an extensive glacial history. All analyzed volcanoes are classified as  
90 stratovolcanoes by the Smithsonian Global Volcanism Program (Global Volcanism Program, 2013).

## 91 **2.1 Edifice Delineation**

92 Although automated algorithms exist to generate volcano edifice boundaries (e.g., Bohnenstiehl et al., 2012;  
93 Euillades et al., 2013), these often create conservative limits around the edifice that ignore lower flanks and volcano-  
94 sedimentary aprons (e.g., O’Hara et al., 2020). We thus follow the method suggested by van Wees et al. (2021) to  
95 delineate edifice boundaries from surrounding topography. Using 30-m Shuttle Radar Topography Mission (SRTM)  
96 Digital Elevation Models (DEMs) (Farr et al., 2007), projected in Universal Transverse Mercator (UTM) with  
97 World Geodetic System (WGS 84), we first generate hillshade, aspect, and local slope rasters of the raw topography.  
98 Lower edifice flanks are generally characterized by slope angles greater than some threshold value (Karátson et al.,  
99 2012); we therefore remove short-wavelength variations of the slope raster by filtering it over a 300 m wavelength  
100 (O’Hara et al., 2020) and contour regions that surpass a 3° slope threshold (van Wees et al., 2021). Using these maps  
101 as visual aids, we then hand-draw boundaries that separate the edifice from surrounding terrain. Afterwards, the  
102 DEMs are clipped using these boundaries to isolate the edifices for morphometric analysis. The planform areas of  
103 edifice boundaries derived using this method range from 30.2 km<sup>2</sup> (Kaitake, New Zealand) to 432.7 km<sup>2</sup> (Muria,  
104 Indonesia).

## 105 **2.2 Edifice Basin Morphology**

106 We analyze edifice basin morphologies with DrainageVolc, a series of scripts modified from TopoToolbox  
107 (Schwanghart and Scherler, 2014), which is designed to investigate volcanic topography through a set of  
108 topography-, drainage-, and channel-based analyses. The metrics considered here are commonly used within  
109 tectonic settings but have not previously been applied to radial drainages. Figure 2 displays an example of our  
110 methods using Ungaran volcano in Indonesia.

111 We first fill sinks in the DEM through TopoToolbox’s preprocessing algorithm (Schwanghart and Scherler, 2014) to  
112 ensure continuous flow to the edifice boundary and extract drainage basins from topography using steepest-descent  
113 flow routing (Fig. 2a). We then perform a series of analyses related to basin geometry. The lengths ( $L$ ) of all basins  
114 draining to the edifice boundaries are calculated by determining mid-point paths between basin divides  
115 perpendicular to the Euclidean distance between the highest and lowest reaches of the basin, irrespective of whether  
116 there is an actual flow channel in this path (Fig. 2d). Assuming basins with total drainage areas ( $A$ ) greater than  
117 some threshold ( $A_T$ ) support overland flow, we explore the correlation between the lengths and drainage areas of  
118 these basins through a power-law regression to derive the Hack’s Law relationship (Fig. 2b) for the edifice as

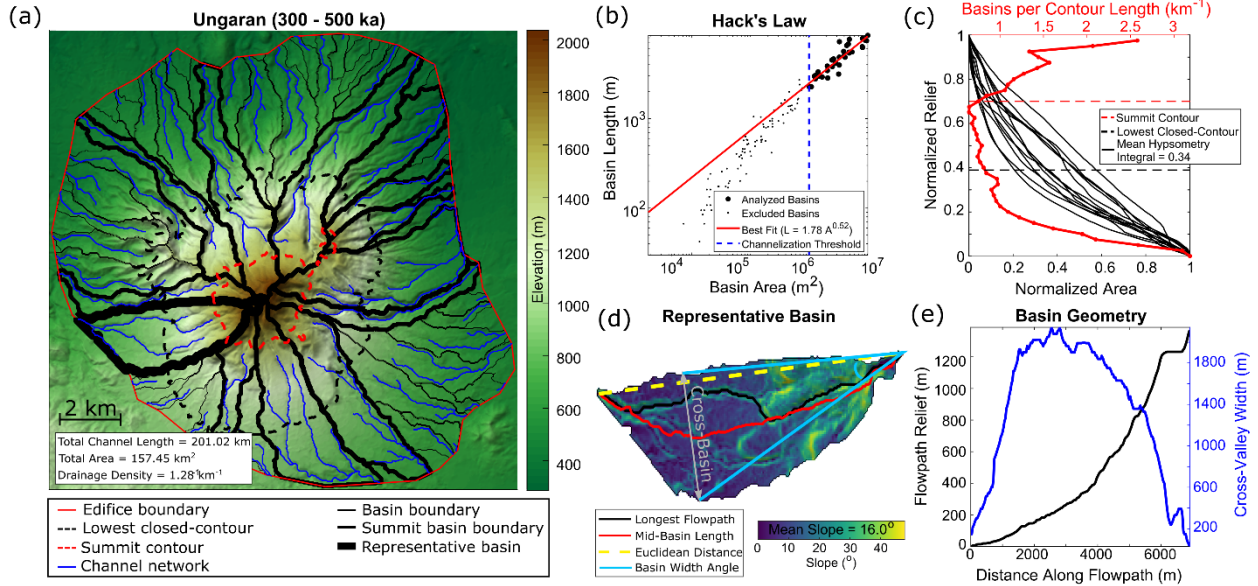
$$119 \quad L = k_a A^H, \tag{1}$$

120 where  $k_a$  and  $H$  are Hack’s coefficient and exponent, respectively (Hack, 1957).  $H$  values are compared across  
121 edifices as this exponent describes general basin geometry, with values of  $\sim 0.47 - 0.6$  typically attributed to  
122 dendritic systems (Hack, 1957; Mueller, 1972). Our Hack’s Law derivation uses basin lengths as opposed to typical  
123 flow path lengths to remove the effects of channel sinuosity and focus explicitly on basin geometry; however, within  
124 the context of our edifice basins, this derivation does not significantly alter our results, and values are thus

125 comparable to those of previous studies (Fig. S1). We also analyze the density of the edifice's channel network by  
 126 extracting flow paths with drainage areas greater than  $A_T$  from the landform, and calculate the edifice-scale drainage  
 127 density as

$$128 \quad DD = \frac{\sum L_c}{A_E}, \quad (2)$$

129 where  $\sum L_c$  is the cumulative sum of all channel lengths and  $A_E$  is the planform area of the edifice's boundary (Fig.  
 130 2a) (Horton, 1945). Using an automated slope-area analysis of basins to determine the drainage area threshold that  
 131 best corresponds with the power-law decrease in slope (Montgomery and Dietrich, 1994) for each edifice  
 132 (Supplemental text; Fig. S2), we find  $A_T$  ranges between 0.32 – 1.62 km<sup>2</sup>, with a mean threshold of 0.85 km<sup>2</sup> (Table  
 133 T1). For consistency across all edifices, we assume a constant drainage area threshold of 1.0 km<sup>2</sup> to delineate  
 134 networks. Sensitivity analysis (Fig. S3) demonstrates that although the selection of  $A_T$  does not significantly impact  
 135 the general behavior of drainage density results, Hack's Law exponent is more sensitive to this choice.



136

137 **Figure 2** – Analyzed basin metrics. **a:** Example from the map of Ungaran volcano (Indonesia), colored lines defined in the  
 138 legend. **b:** Hack's Law relationship between basin areas and lengths. Black circles are basins used in the power-law analysis,  
 139 black dots are excluded basins; blue-dashed line is the drainage area threshold ( $A_T$ ; 1.0 km<sup>2</sup>) for channelization. **c:** Scaled edifice  
 140 metrics. Red line shows normalized number of basins along elevation contours. Black lines are summit basin hypsometry curves.  
 141 **d:** Local slope and geometry values of representative basin (thick black line in 2a). Gray double-arrow represents cross-basin  
 142 direction (i.e., the extent of the basin) perpendicular to the Euclidean basin length. **e:** Cross-basin values along basin shown in 2d.  
 143 Black line is relief along the flowpath, blue line is cross-valley width.

144 Afterwards, we calculate mean values of basin geometries on each edifice. Rather than analyze the geometry of all  
 145 basins that exist on a volcano, we limit our analysis to larger basins that best characterize the edifice's drainage, and  
 146 thus its dismantling. These large characteristic basins may be determined using a variety of methods, such as  
 147 through an arbitrary number or percentage of basin sizes, using the basins that are within some radial distance of the  
 148 edifice's peak, or determining basins that extend to some portion of the edifice's height. Determining characteristic

149 basins by an arbitrary number or percentage of basin sizes may introduce bias as the population of basins drastically  
 150 varies between edifices (Fig. 8a), whereas determining characteristic basins by radial distance from the edifice's  
 151 peak introduces geometric constraints as edifice shapes often deviate from the textbook symmetric, single-peaked  
 152 edifice, instead developing large, irregular summit regions that are defined by high topography and multiple peaks  
 153 (e.g., Karátson et al., 1999; Grosse et al., 2012). As slope (and thus elevation) is an essential component of erosion  
 154 and basin development (Hack, 1957; Flint, 1974), we define characteristic basins as those that reach the edifice's  
 155 summit region. However, we note that defining characteristic basins based on radial distance can produce different  
 156 trends (Fig. S4) and may be more appropriate for some of our analyzed metrics (Section 5.3).

157 Generating a series of elevation contours along the edifice at intervals of 2.5% of the edifice's relief, we calculate  
 158 the number of basins that intersect each contour, normalized by the contour's length (Fig. 2c, red line). For all  
 159 edifices, we define the edifice's summit as the upper 30% of the edifice's relief, and thus consider the basins that  
 160 reach this summit region (referred here as *summit basins*) as those that best characterize the edifice's drainage  
 161 development. We then determine summit basin numbers, mean basin slopes (Fig. 2d), basin lengths ( $L_B$ ; Fig. 2d, red  
 162 line), basin reliefs (Fig. 2e, black line), and maximum cross-basin widths ( $W_B$ ; Fig. 2e, blue line). To compare  
 163 values across edifices of varying sizes, summit basin numbers are normalized by the length of the summit contour  
 164 (Fig. 2c) and basin reliefs are normalized by the relief of the entire edifice. We also utilize the radial nature of  
 165 edifices to generate normalized values of basin length ( $L'_B$ ) and width ( $W'_B$ ) as

$$166 \quad L'_B = \frac{L_B}{L_E}, \quad (3)$$

167 and

$$168 \quad W'_B = 2 \tan^{-1} \left( \frac{W_B/2}{L_{W_B}} \right), \quad (4)$$

169 respectively, where  $L_E$  is the edifice's effective radius, defined as the radius of the circle with the same planform  
 170 area ( $A_E$ ) as the edifice's boundary ( $L_E = \sqrt{A_E / \pi}$ ), and  $L_{W_B}$  is the distance from the highest point within a basin to  
 171 where the basin is widest.  $W'_B$  thus converts basin widths into an angle relative to the summit (Fig. 2d, light blue  
 172 lines). Mean values of these quantities are then calculated for each edifice.

173 We also calculate mean summit basin hypsometry integrals for each edifice (Strahler, 1952; Fig. 2c, black lines).  
 174 Individual basin hypsometry curves ( $H_C$ ) are derived by counting the number of basin pixels  $N_{P_B}$  at or above  
 175 normalized elevation values ( $\dot{Z}$ , ranging from 0 to 1); afterwards, these values are normalized by the total number of  
 176 basin pixels ( $N_{P_{Tot}}$ ) as

$$177 \quad H_C(\dot{Z}_I) = \frac{N_{P_B}(\dot{Z} \geq \dot{Z}_I)}{N_{P_{Tot}}}, \quad (5)$$

178 where  $I$  is a counter over normalized elevation values from 0 to 1. Hypsometry integrals of each basin are calculated  
 179 as the positive integration over the curves from eq. (5). These are also averaged for each edifice.

### 180 2.3 Edifice Landform Morphology

181 As well as studying the temporal evolution of drainages on edifices, we also consider the broad geometry of the  
182 volcanoes. Grosse et al. (2009, 2012) developed the initial MorVolc algorithm in IDL, which quantifies edifice  
183 morphologies through a series of size, shape, slope, orientation, peak, and summit parameters. Using the same  
184 framework as DrainageVolc, we redeveloped the IDL code in Matlab, also utilizing the TopoToolbox DEM analysis  
185 package (Schwanghart and Scherler, 2014). Both DrainageVolc and the updated MorVolc scripts are available for  
186 use on GitHub ([https://github.com/danjohara/Volc\\_Packages](https://github.com/danjohara/Volc_Packages)).

187 We analyze simple edifice geometry measurements with this updated version of MorVolc, including effective  
188 radius, height, height-radius ratio, and mean slope of the main flank (edifice region between the lowest closed-  
189 contour that encompasses the edifice and the summit contour, Fig. 2a). We also quantify the mean contour ellipticity  
190 and irregularity indices of the main flank from the previously-computed contours. The ellipticity index ( $EI$ )  
191 describes the elliptical nature of the edifice elevation contours, and is defined as

$$192 \quad EI = \frac{\pi(L_M/2)^2}{A_C}, \quad (6)$$

193 where  $L_M$  is the length of the major axis of a best-fitting ellipse through the contour and  $A_C$  is the area enclosed by  
194 the contour (Grosse et al., 2012). The irregularity index ( $II$ ) describes divergence of the contour from a smooth  
195 ellipse as

$$196 \quad II = di_{contour}(di_{ellipse} - 1), \quad (7)$$

197 where  $di$  is the dissection index, defined as

$$198 \quad di = \frac{P_C}{2A_C} \sqrt{A_C/\pi}, \quad (8)$$

199 with  $P_C$  and  $A_C$  being the perimeter and area of the contour, respectively (Grosse et al., 2012). Finally, we also  
200 incorporate new measurements within MorVolc, including the slope variance of the entire edifice (standard  
201 deviation of all slope values divided by the mean slope, similar to roughness), as well as a minimum eroded volume  
202 estimate. Eroded volume is estimated from a convex-hull reconstruction of the edifice, using the methodology  
203 described in O'Hara and Karlstrom (2023), in which the footprints of individual elevation contours along the edifice  
204 are altered to remove concave regions (assuming they represent incised topography), thus creating convex polygons.  
205 Polygons are then interpolated in three dimensions to create a simplified, reconstructed edifice. Afterwards, the  
206 current topography is subtracted from the reconstructed edifice and positive values (i.e., areas having been eroded)  
207 are integrated to estimate the volume of eroded material. Finally, eroded volume is normalized as a percent relative  
208 to the total reconstructed volume.

209 Edifice landform and basin metrics that are based on average values (main flank mean slope, mean contour  
210 irregularity index, mean contour ellipticity index, as well as mean summit basin hypsometry, length, width, relief,  
211 and slope) have standard deviations of the sampled population that are presented as vertical bars in Figs. 3 – 4. Other

212 metrics (edifice height, radius, height-radius ratio, slope variance, normalized eroded volume, Hack's Law exponent,  
213 drainage density, and normalized number of summit basins) are singular values for each edifice and thus do not have  
214 associated standard deviations. Potential deviations of these values relate to the edifice's boundary, summit  
215 designation, DEM source, or imposed drainage area threshold (Grosse et al., 2012; O'Hara et al., 2020; van Wees et  
216 al., in review; Supplemental text).

## 217 **2.4 Edifice Ages**

218 To explore morphological evolution through time, we correlate edifice landform and drainage basin metrics to  
219 volcano ages of activity. We thus compile known eruption records of each volcano, with ages ranging from present  
220 to early Pleistocene (Table T2). Volcanoes often have complex surface evolutions, with lifespans of activity that  
221 range 100-1000 kyrs and characterized by episodes of stochastic growth interspersed with periods of erosion during  
222 quiescence (e.g., Karátson et al., 1999; Lahitte et al., 2012). Furthermore, episodes of activity are often constrained  
223 to localized regions of the edifice and thus do not fully resurface the entire landform (e.g., Civico et al., 2022).  
224 Similarly, erosion across the edifice is typically non-uniform as local conditions are dependent on the age and type  
225 of activity, as well as microclimates (e.g., Ferrier et al., 2013; Pierson and Major, 2014; Thouret et al., 2014; Ricci et  
226 al., 2015).

227 Despite the spatial and temporal heterogeneities of activity and erosion, we argue that a generalized morphologic  
228 age of an edifice may be derived that quantifies the erosional state of the landform and relates to the edifice's  
229 lithologic age. To account for the time differences between short-term events and the cumulative long-term history  
230 on morphology, we define an edifice's age as a single value using the log-mean between the most recent eruption  
231 and oldest date of activity. This definition thus accounts for the span of temporal magnitudes; however, we note that  
232 using linear-mean ages produce similar results (Fig. S5) and recognize that other definitions of an edifice's  
233 morphologic age are plausible (e.g., the time since the last eruption; Fig. S6). Afterwards, we analyze the temporal  
234 evolution of edifice morphologies by fitting logarithmic relationships between edifice age and morphometric  
235 parameters. Some volcanoes (Sumbing, Bamus, and Ulawun) have poorly-documented histories (only the most  
236 recent eruption has been dated) and are therefore excluded from the regression. Conversely, Likuruanga is known to  
237 have erupted only during the Pleistocene and is incorporated in the analysis.

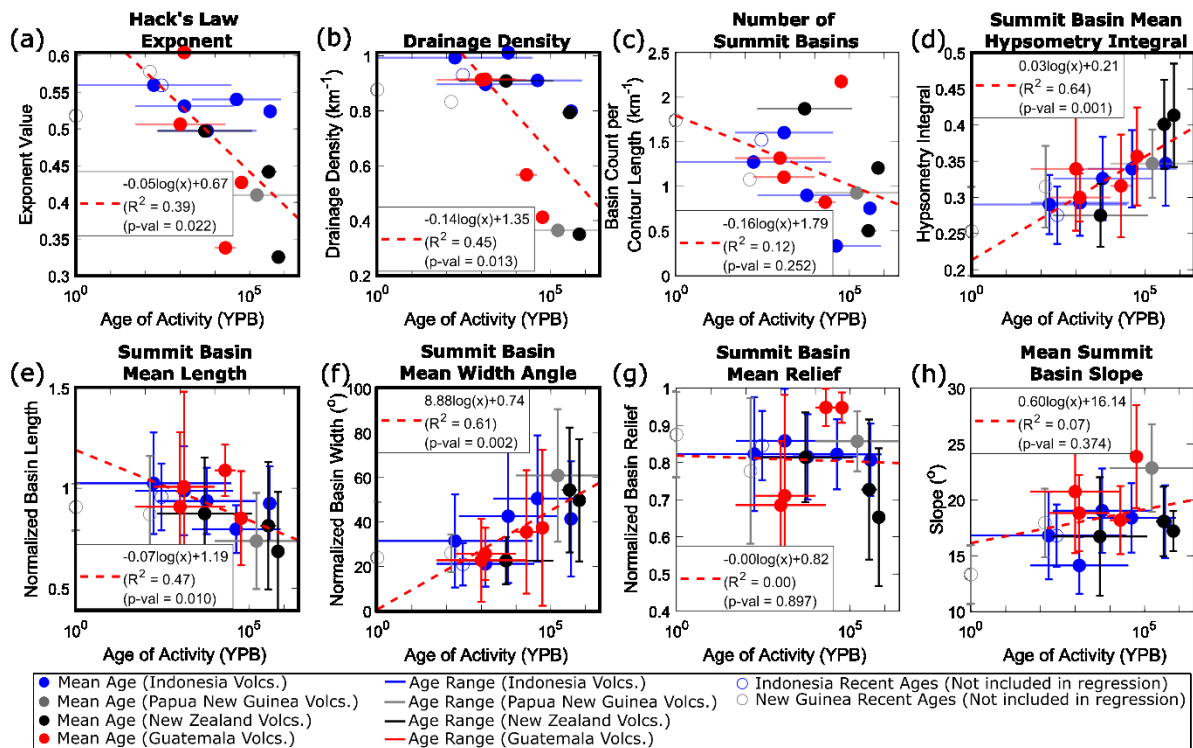
## 238 **3.0 Results**

239 We find trends between stratovolcano age and our morphometry metrics through time (Figs. 3-4; Supplemental  
240 Table T3). Considering all metrics, we find that edifice height, mean ellipticity index, normalized eroded volume,  
241 Hack's Law exponent, drainage density, mean summit basin hypsometry integral, normalized basin length, and  
242 normalized basin width have  $R^2$  values ranging 0.39 – 0.77 and correlation p-values  $\leq 0.05$ . This list expands to  
243 include effective edifice radius and mean irregularity index by removing a notable outlier (Muria, Indonesia; Fig. 4b,  
244 4e), suggesting all of these metrics provide quantitative measures to characterize the overall maturity of the edifice.  
245 Other metrics have weaker correlation values (0 – 0.25) and are statistically insignificant (p-values  $> 0.1$ ), and thus  
246 may be more sensitive to the initial edifice geometry or other processes that alter edifice morphology, or that age is  
247 not a significant factor for these metrics. Muria (the noted outlier for effective edifice radius and irregularity index),

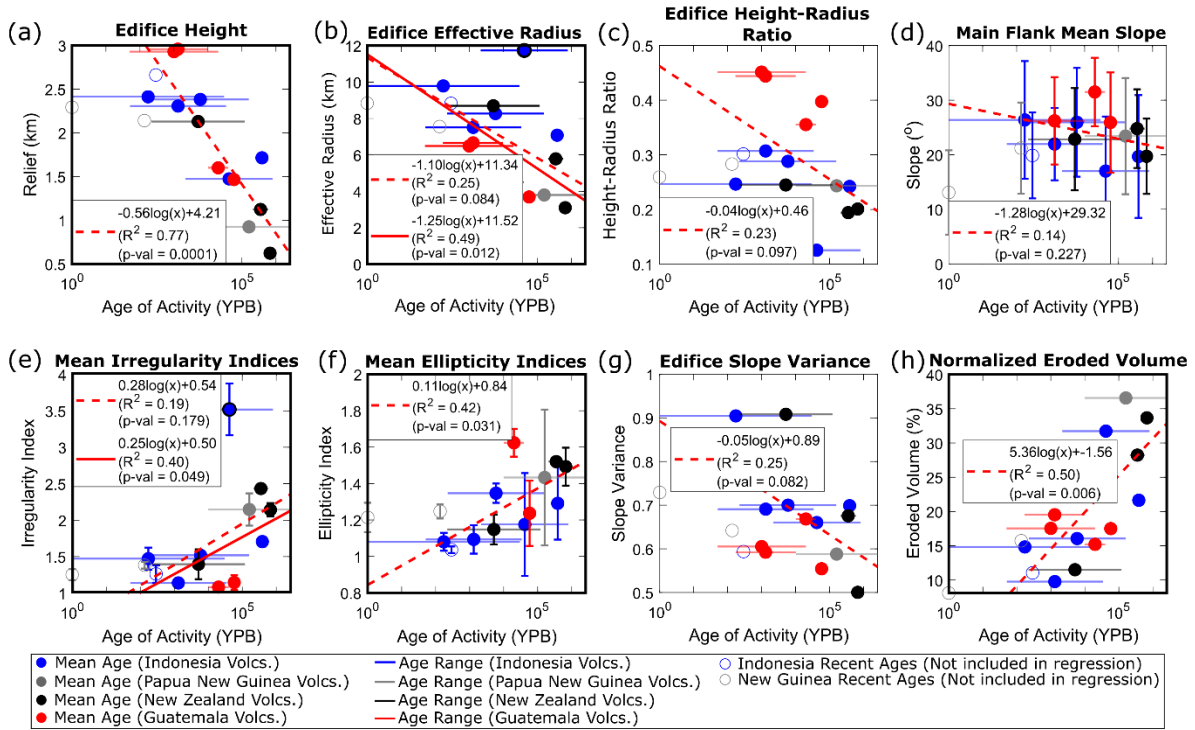


248 has an extensive volcanic history (from ~ 800 ka to 2 ka; McBirney et al., 2003; Global Volcanism Program, 2013)  
 249 and a morphology characterized by two broad fluvial networks on opposite flanks that are deeply incised into the  
 250 landform and may be associated with breached craters or flank collapses (Fig. 1a), suggesting this edifice may not fit  
 251 into the simple, radial volcano expectation of our dataset. We also note that due to the geometries that Acatenango  
 252 and Atitlán share with their sister volcanoes (Fuego and Tolimán, respectively; Fig. 1d), and our imposed definition  
 253 of an edifice's main flank (region between the lowest closed-contour and upper 30% of the edifice's height),  
 254 irregularity and ellipticity values could not be derived for these volcanoes.

255 Of the statistically-significant metrics related to edifice drainage morphology, mean summit basin hypsometry  
 256 integral and normalized width increase through time, whereas Hack's Law exponent, drainage density, and mean  
 257 summit basin normalized length decrease (Fig. 3). Similarly, considering statistically-significant metrics related to  
 258 the edifice as a primary landform, mean irregularity index, mean ellipticity index, and convex-hull based eroded  
 259 volumes increase with age, while edifice height and effective radius decrease with age (Fig. 4).



260  
 261 **Figure 3** – Temporal relationships of drainage basin morphology metrics. Colors correspond to volcanic region. Horizontal lines  
 262 are edifice age ranges of activity, with filled circles representing log-mean age. Vertical lines represent one standard deviations of  
 263 values (where appropriate). Red-dashed lines and equations characterize logarithmic regressions; open circles are excluded from  
 264 the regression due to age constraints. Thick black border highlights relationships with  $R^2 > 0.35$ .



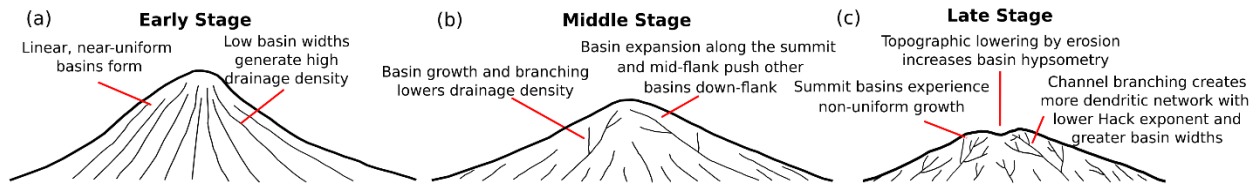
265  
 266 **Figure 4** – Temporal relationships of landform morphology metrics. Colors and symbols are same as those described in Fig. 3.  
 267 Solid red lines in (b) and (e) are secondary regressions with outlier (Muria) excluded. Thick black border highlights relationships  
 268 with  $R^2 > 0.35$ .

269 **4.0 Discussion**

270 **4.1 Generalized model for edifice degradation**

271 The evolution of stratovolcanoes as primary landforms and the drainage basins that erode them are inextricably  
 272 linked. Our results thus establish a new framework for evaluating volcanic edifices by considering both the landform  
 273 and its drainage systems. This evolutionary model expands on stages previously defined qualitatively (Ollier, 1988)  
 274 and follows similar drainage evolution to that observed in badlands (Schumm, 1956).

275 Erosion of a stratovolcano can be described within the context of our metrics by considering a simplified, conical  
 276 edifice (Fig. 5). In the initial stages of erosion (Fig. 5a, equivalent to ~10% normalized eroded volume in Fig. 4h),  
 277 narrow (~20° normalized width angle) and uniform (normalized mean length near 1) drainages form that extend  
 278 from the summit region to the lower flanks (i.e., ‘parasol ribbing’; Ollier, 1988), giving a high drainage density (~1  
 279  $\text{km}^{-1}$ ) and Hack’s Law exponent (~0.6).



280  
 281 **Figure 5** – Conceptual model of edifice dissection based on interpretation of temporal morphologic trends shown in Figs. 3 – 4.  
 282 Thin black lines represent drainage systems.

283

284 As the edifice degrades to 30-40% normalized eroded volume (Fig. 4h) on 10-100 kyr timescales (Fig. 5b-c), both  
285 its height and area decrease; however, height decreases faster, leading to a decrease in height-radius ratios. The  
286 erosion of the edifice is accompanied by drainage basin growth, with summit basins expanding azimuthally along  
287 the edifice to normalized basin widths of 40-60°, pushing the headwaters of other basins down the edifice flanks.  
288 Furthermore, as summit basins expand, they incise into the edifice flanks and develop a more dendritic structure  
289 associated with lower drainage density ( $\sim 0.5 \text{ km}^{-1}$ ) and Hack's Law exponent ( $\sim 0.4$ ). This is accompanied by non-  
290 uniform summit basin growth that causes normalized basin lengths to decrease below 1.

291 As the edifice erodes, processes occur over varying scales to alter general edifice morphology: 1) over the entire  
292 edifice, erosion-driven topographic lowering occurs faster than horizontal areal loss of the edifice, creating a flatter  
293 landform; and 2) at the scale of a basin, incision carves into the initially-planar flanks of the edifice, steepening  
294 surrounding valley walls and increasing contour irregularity. The relationship between basin-scale incision and  
295 edifice-scale flattening is recorded through summit basin hypsometry integrals, with increasing values suggesting  
296 that edifice-scale flattening is the dominant process. This leads to a scale-dependent behavior in edifice morphology  
297 – although the edifice as a landform is becoming flatter, incision causes topography to steepen locally. Previous  
298 studies (e.g., Karátson et al., 2012; Dibacto et al., 2020; Ollier, 1988) suggest this simultaneous behavior causes the  
299 edifice to lose its conical, single-peaked nature over longer ( $> 1 \text{ Myr}$ ) timescales, developing high-relief drainage  
300 divides over an extended summit region that support binary basin competition as the edifice erodes to the same relief  
301 as the surrounding terrain. Furthermore, we note that the decrease in edifice area through time differs from the  
302 expectation of a sedimentary apron around the edifice that increases in area as the edifice erodes. Since edifice  
303 boundaries are consistently defined in-part by a  $3^\circ$  topographic slope threshold, this suggests that on the 100 kyr  
304 scale, sediment is not depositing at the edifice's base, but is being evacuated from the vicinity of the edifice, likely  
305 through fluvial transport. The loss of sedimentary apron and overall decrease in edifice planform area was also  
306 suggested by Ollier (1988) as an edifice transitions from its 'intact' stage to 'planèzes' stage.

307 This conceptual model represents a generalized view of edifice degradation, as a variety of processes (both volcanic  
308 and erosional) can impact an edifice's morphology throughout its lifespan. Furthermore, other climate conditions not  
309 considered here (e.g., glaciers, arid environments) are expected to alter the patterns and rates of basin evolution.  
310 Nonetheless, we propose that, barring major events that significantly alter topography, stratovolcano degradation by  
311 fluvial processes generally follows the model presented here.

#### 312 **4.2 How do basins compete on radial structures?**

313 Our results suggest that drainages on radial structures are highly dynamic. From initially-uniform basin geometries,  
314 preferential erosion causes basins near the summit to become more dominant and expand, forcing other basins  
315 down-flank and generating a 'topographic hierarchy', with higher-order basins spanning the entire flank of the  
316 edifice and lower-order basins occurring on lower sections, analogous to inferred basin evolution on linear fault  
317 blocks (Talling et al., 1997). This hierarchy of basin ordering is a direct product of non-uniform basin development

318 over the edifice that contributes to the preservation of less-eroded portions of the lower flanks (i.e., planèzes; Ollier,  
319 1988).

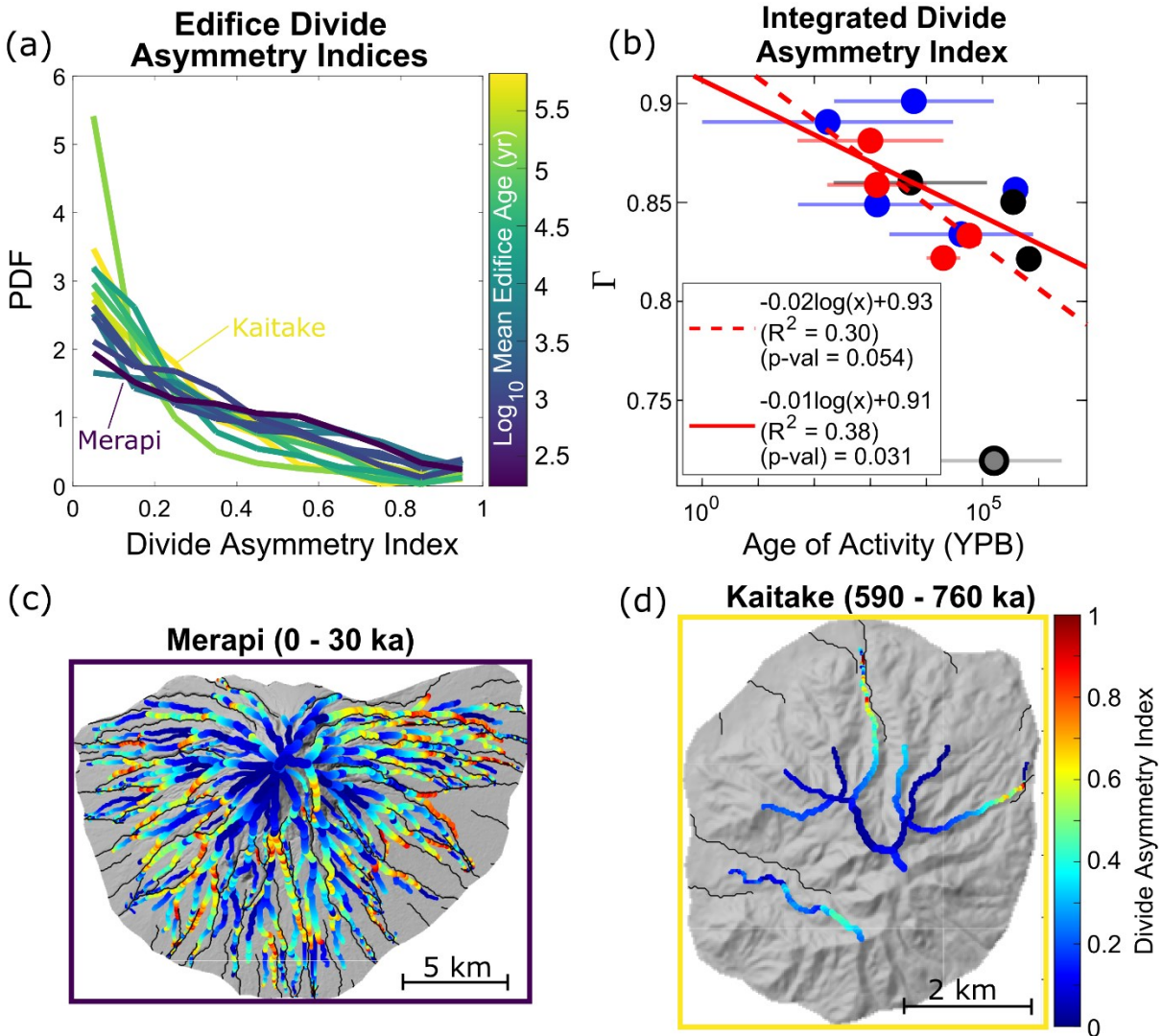
320 Non-uniform basin development and transience is a natural component of landscape evolution (e.g., Hasbargen and  
321 Paola, 2000); however, various factors (both volcanic and non-volcanic) can influence erosional patterns and  
322 accentuate basin growth across volcanic edifices. These may include 1) local slope changes associated with  
323 magmatic intrusions (e.g., Wicks et al., 2002; Biggs et al., 2010; Castro et al., 2016) or mass-wasting (e.g., Ui and  
324 Glicken, 1986; Shea and van Wyk de Vries, 2008); 2) variable volcanic eruption activity that increase sediment  
325 loads (Hayes et al., 2002; Pierson and Major, 2014), alter infiltration and rock erodibility (e.g., Wells et al., 1985;  
326 Sklar and Dietrich, 2001; Jefferson et al., 2010), or remove bedrock through scouring by pyroclasts (Gase et al.,  
327 2017) or melting by lava flows (i.e., thermal erosion; Kerr, 2001) during deposition; 3) non-uniform changes in  
328 overland flow and stream power associated with breached craters (e.g., Karátson et al., 1999) or edifice-scale  
329 precipitation gradients (e.g., Ferrier et al., 2013); and 4) downstream alterations to drainage channels that migrate  
330 upstream as a propagating incision wave (i.e., knickpoints; Kirby et al., 2003; Cook et al., 2013; Perron and Royden,  
331 2013). The long-term compilation of such processes helps drive non-uniform erosion across the edifice, which in  
332 turn encourages divide migrations and changes in basin size and geometry. More specifically, basins that exhibit  
333 higher erosion rates would tend to expand at the expense of their neighboring basins and potentially become the  
334 dominant basins, while lower erosion rates will cause other basins to shrink and their boundaries to migrate further  
335 down the edifice's flank.

336 The morphology of drainage divides is sensitive to differences in erosion between neighboring basins and can thus  
337 be used to characterize basin competition. We quantify basin geometry unsteadiness through an exploration of  
338 divide stability using the *divide asymmetry index* (*DAI*; Forte and Whipple, 2018; Scherler and Schwanghart, 2020),  
339 calculated as the positive difference in hillslope relief (vertical distance between the ridge and nearest channel)  
340 across a divide and normalized by the sum of hillslope reliefs, ranging between 0 (symmetric) and 1 (asymmetric).  
341 We limit our analysis to only consider divides that correspond to fluvial basins (i.e., have drainage areas > 1.0 km<sup>2</sup>  
342 (Scherler and Schwanghart, 2020).

343 Divide mobility is expressed using probability density functions (PDFs) of *DAI* for all volcanoes (Fig. 6a). A clear  
344 temporal trend emerges – older volcanoes have larger distributions clustered around lower (< 0.4) *DAI* that rapidly  
345 decrease with increasing *DAI*; while younger volcanoes show monotonically-decreasing distributions, with fewer  
346 normalized populations of low-*DAI* and greater normalized populations of high-*DAI* values compared to older  
347 volcanoes. Integrating these PDFs into single values (referred to here as  $\Gamma$ ; Fig. 6b) shows a moderate correlation  
348 with age ( $R^2 = 0.38$ ) with the removal of Likuruanga (Papau New Guinea) as an outlier, which may be associated  
349 with a breached crater (Fig. 1b).

350 Combined with basin morphology trends (Fig. 3), this suggests younger volcanoes have basins with more uniform  
351 planform geometries and less-stable basin configurations. As the edifice erodes, basin planform geometries become  
352 less uniform, but develop more stable configurations as evidenced by the greater symmetry of hillslope relief across

353 divides. The relationship between basin non-uniformity and stability can be observed spatially by comparing *DAI*  
 354 values between Merapi (youngest) and Kaitake (oldest) volcanoes (Fig. 6c-d). Highest *DAI* values on both  
 355 volcanoes generally occur at the mid- and lower-flanks of the volcano, suggesting basin expansion occurs mainly  
 356 azimuthally along edifice flanks, rather than across the edifice summit. This spatial analysis highlights the process  
 357 that generates topographic hierarchy – by expanding azimuthally, basin growth drives less-dominant basins down-  
 358 flank through a zippering process, creating drainages with tapered geometries along the lower flanks.



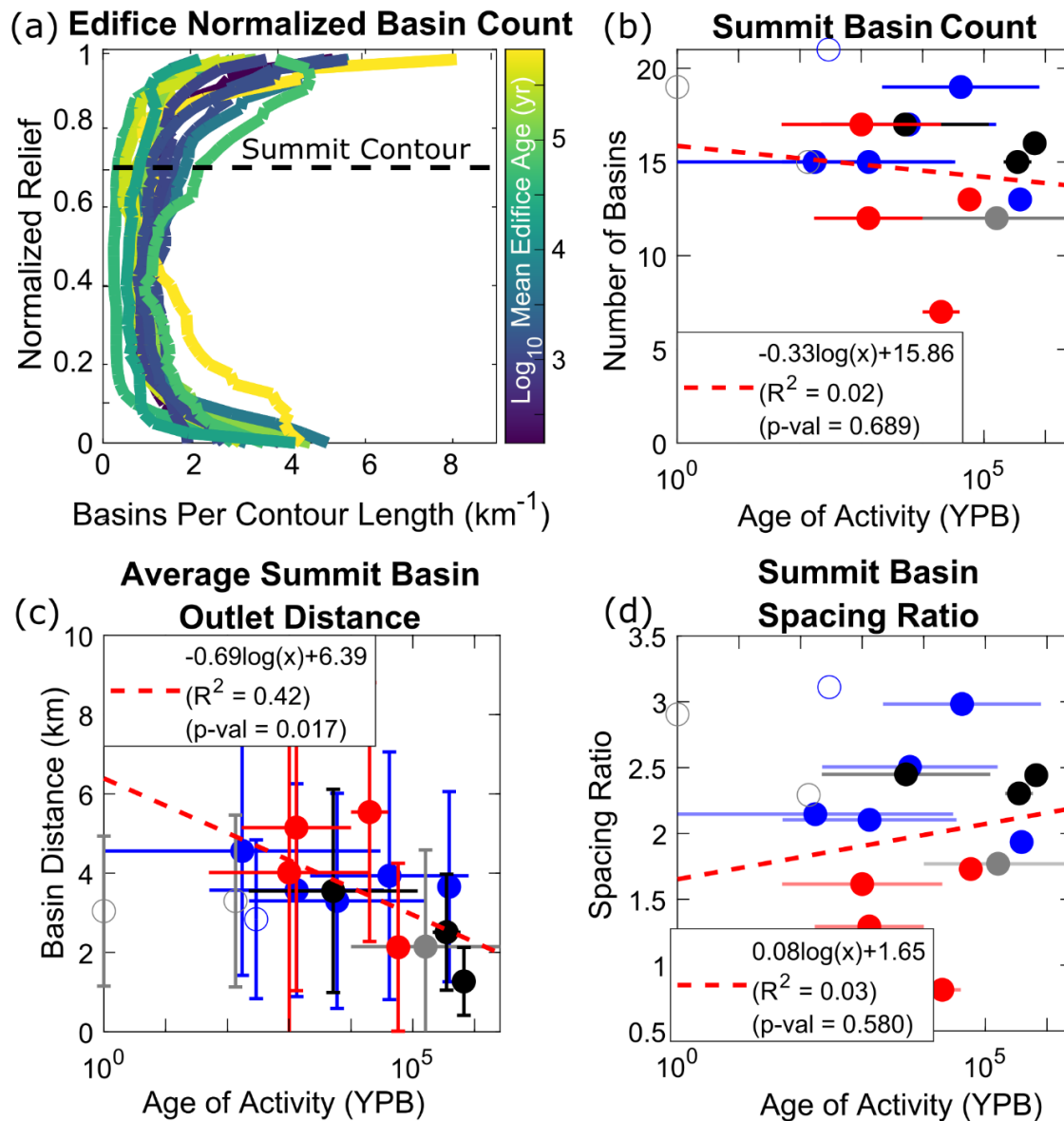
359

360 **Figure 6 – a:** Probability density functions (PDFs) of volcano divide asymmetry indices (*DAI*); colors correspond to log-mean  
 361 edifice ages. **b:** Integral of PDFs (*I*) compared to edifice age. Colors and symbols are the same as Fig. 4. **c-d:** *DAI* values for (c)  
 362 Merapi (Fig. 1a) and (d) Kaitake (Fig. 1c) at the divides. Background images are hillshade of topography, black lines are edifice  
 363 channel network. Borders are colored with respect to Fig. 6a color scale.

### 364 4.3 Edifice basin widths and spacing

365 Our results show that edifices experience the same morphologic trends when considering the number of basins along  
 366 edifice relief (Fig. 7a): lower flanks are characterized by normalized basin numbers between 2–5 km<sup>-1</sup>, main flanks  
 367 are characterized by relatively consistent normalized basin numbers < 2 km<sup>-1</sup>, while the normalized basin numbers

368 increase near the summit (upper 30% of the edifice). This trend appears to occur largely independent of age, even  
 369 within the upper flank (as demonstrated by a low  $R^2$  value of 0.12 at the summit contour, Fig. 3c), suggesting that  
 370 this morphologic trend is a direct consequence of the conical nature of volcanoes. Furthermore, non-normalized  
 371 summit basin numbers also demonstrate a weak temporal trend, both at the upper 30% height designation (Fig. 7b)  
 372 as well as other percentages (Fig. S7). This suggests that basins that initially form on the summit region may retain  
 373 their topographic position as the edifice erodes. However, Fig. 3f demonstrates that these basins still widen through  
 374 time, to a width angle of  $\sim 60^\circ$ , though further analysis on older volcanoes is needed to explore whether this persists  
 375 on the Myr-timescale.



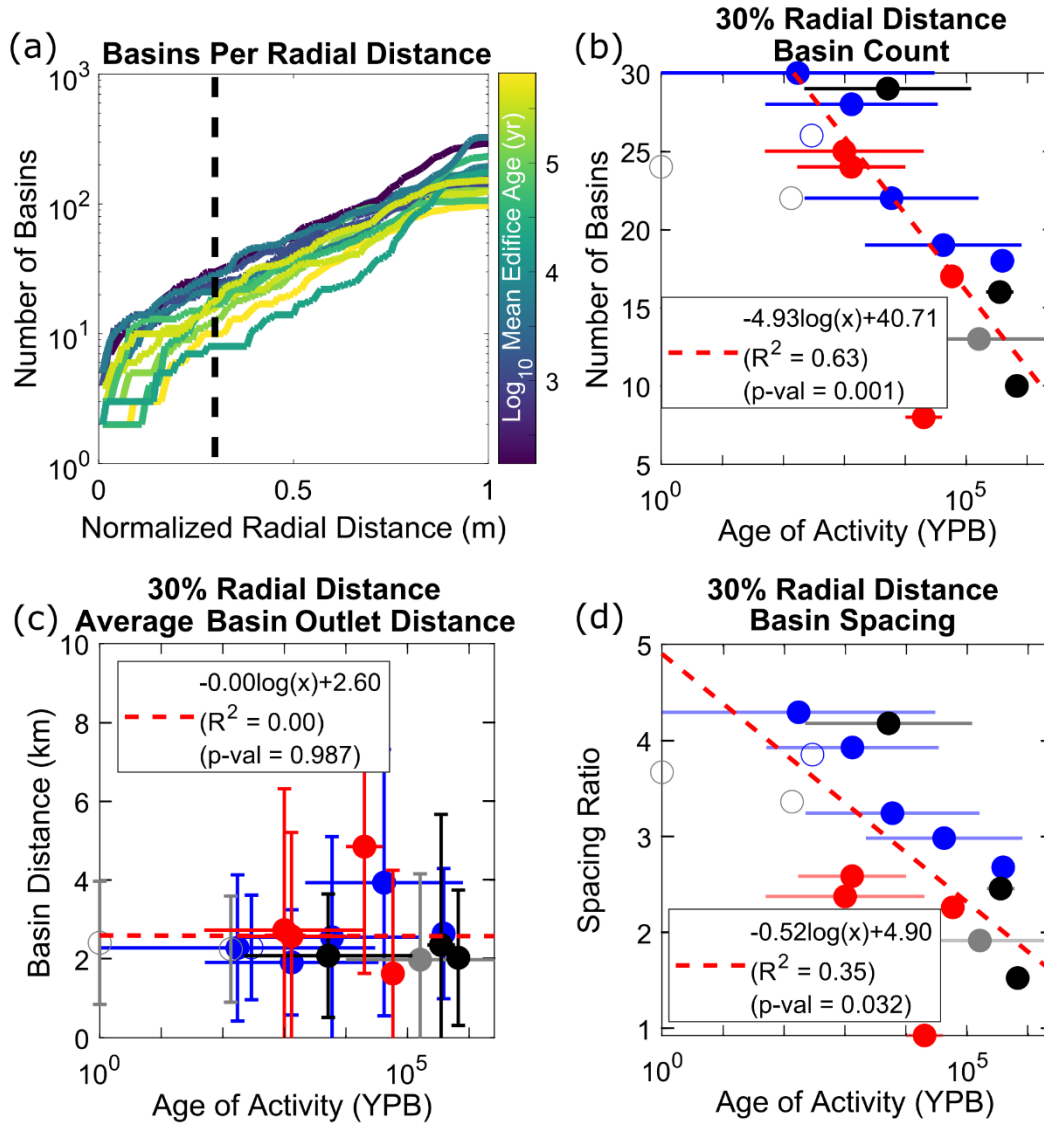
376 **Figure 7 – a:** Normalized number of basins along normalized relief for each volcano; colors are log-mean edifice age. **b:** Non-  
 377 normalized number of summit basins (defined by the upper 30% of the edifice’s height; black-dashed line of a) compared to log-  
 378 mean edifice age. **c:** Average along-perimeter summit basin distance compared to edifice age. **d:** Summit basin spacing ratio  
 379 (data from Fig. 4b divided by data from c) compared to edifice age. Colors and symbols in b-d are the same as Fig. 3.  
 380

381 An apparent contradiction occurs when comparing mean summit basin width angles to the number of summit basins.  
382 If all summit basins reached a width angle of  $\sim 60^\circ$ , it would be expected that only  $\sim 6$  basins would exist at the  
383 summit; however, Fig. 7b shows that the number of basins that reach the summit on most edifices is greater than 10.  
384 This difference is a consequence of radial drainage basins achieving their maximum widths at different heights  
385 relative to the height of the edifice, such that basin widths are normalized by different distances from the summit.  
386 Indeed, as discussed in Section 4.2, divide asymmetry is most frequent in the mid- and lower-flanks of the edifice  
387 (Fig. 6), thus accommodating largest basin widths at different sections of the flank.

388 If the number of basins that reach the summit is time invariant, how does this translate to the circumferential spacing  
389 of their outlets at the base of the edifice? Hovius (1996) compiled the ratio between mountain belt half-widths  
390 (distance between the major divide and mountain front,  $W_M$ ) and distances between major drainage basin outlets  
391 (those that reach the major divide;  $s$ ) in 11 mountain ranges globally, and determined a globally-averaged spacing  
392 ratio ( $W_M / s$ ) of  $\sim 2$ -3. We perform a similar analysis by dividing edifice effective radii by the average along-  
393 perimeter spacing between summit basin outlets. Figs 4b and 7c show that while edifice effective radii decrease  
394 through time, so does the average perimeter distance between summit basin outlets. These behaviors thus combine  
395 to produce summit basin spacing ratios of  $\sim 1 - 3$  (Fig. 7d), consistent with Hovius (1996) as well as modeling  
396 studies of drainage patterns (Habousha et al., 2023). This suggests that while summit basins azimuthally expand  
397 their widths, the edifice is also decreasing in area as the landform erodes, thus decreasing the distances between  
398 summit basin outlets.

399 However, a different behavior emerges when considering basins by their radial distance relative to the edifice's peak  
400 (Fig. 8), which is more sensitive to the areal expansion of basins along the edifice's flank. Plotting the non-  
401 normalized number of basins as a function of radial distance (normalized by maximum radius for each edifice) and  
402 time shows a clear temporal trend (Fig. 8a), with younger edifices having more basins along all sections of the  
403 volcano (as schematized in Fig. 5). This trend becomes more apparent through the logarithmic regression between  
404 edifice age and the number of basins that exist at 30% radial distance from the peak (Fig. 8b), with other normalized  
405 distances showing the same behavior (Fig. S8). Conducting a similar outlet perimeter-distance analysis on these  
406 basins shows that the average distance between basin outlets is relatively constant at  $\sim 2$  km (Fig. 8c), giving a  
407 temporal decrease in basin spacing ratios ( $R^2 = 0.35$ , Fig. 8d). This relationship suggests a dynamic in radial  
408 drainage evolution related to landform geometry. Combined with other metrics, our results suggest that as the  
409 edifice erodes and loses planform area through time, very small basins on the edifice's lower flanks likely become  
410 erased while more dominant basins widen on the mid flank, thus causing basins that exist within 30% radial distance  
411 of the edifice's summit to retain an approximately constant outlet distance along the shrinking perimeter.





412

413 **Figure 8 – a:** Non-normalized number of basins as a function of normalized distance from the edifice’s peak; colors are log-  
 414 mean edifice age, black-dashed line represents 30% normalized radial distance from the edifice’s peak (basins used for plots in  
 415 b-d). **b:** Non-normalized number of basins compared to log-mean edifice age. **c:** Average along-perimeter basin distance  
 416 compared to edifice age. **d:** Basin spacing ratio (data from Fig. 4b divided by data from c) compared to edifice age. Colors and  
 417 symbols in b-d are the same as Fig. 3.

418 **4.4 Radial drainage basin area-length relationship**

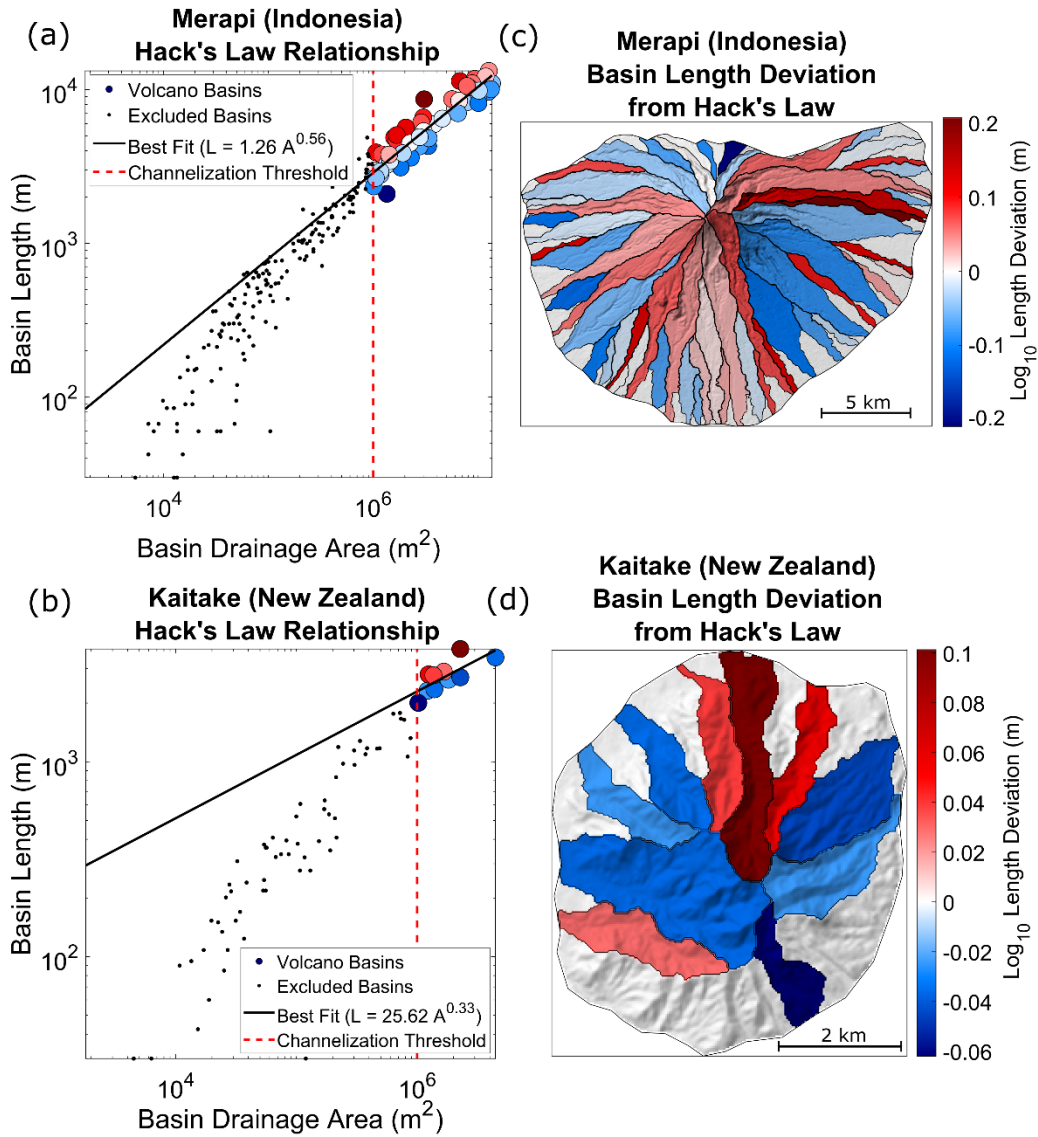
419 As a final observation for volcanic edifice drainage basins, we consider basin geometries in reference to Hack’s  
 420 power-law relationships between basin areas and lengths (Hack, 1957). Analyzing Hack’s Law regressions for  
 421 Merapi and Kaitake (Fig. 9), the relationships between spatial location and basin geometries become apparent. On  
 422 Merapi, basins less than  $10^5 \text{ m}^2$  do not conform to the same power-law trend as those greater than  $10^5 \text{ m}^2$ , whereas  
 423 on Kaitake this break occurs at  $10^6 \text{ m}^2$ . These smaller basins are constrained to the lowest regions of the edifices’  
 424 flanks and likely correspond to non-channeled surfaces. Of those considered for the Hack’s Law regression, the  
 425  $\log_{10}$  basin length deviation ( $D_L$ ) from the power-law is calculated as



426  $D_L = \log_{10}(L_H(A)) - \log_{10}(L),$  (9)

427 where  $L_H$  is the basin length of the Hack's Law regression from a given basin's area ( $A$ ), and  $L$  is the basin's length.  
428 As expected from the geometric relationship, basins that fall below the power-law regression ( $D_L < 0$ ) are wider,  
429 and those that are above the power-law regression ( $D_L > 0$ ) are narrower.

430 Calculating  $D_L$  for basins with areas greater than our imposed channelization threshold ( $1.0 \text{ km}^2$ ), one clear  
431 observation is the presence of highly-elongated basins on Merapi that exist on the mid- to upper-flanks and have  $D_L$   
432 values  $> 0.15$  (Fig. 9c). These basins appear wedged or pinched between larger basins and would be expected to not  
433 have as much growth potential compared to their wider neighbors. Elongated basins also exist on Kaitake; however,  
434 they do not have as high of a deviation (maximum  $D_L \approx 0.1$ ; Fig. 9d). This may be a product of the lower number of  
435 basins that exist on Kaitake, the overall lower amount of drainage area that Kaitake basins occupy, or an evolution  
436 of basins towards more consistent patterns, thus decreasing the amount of variability from the power-law  
437 relationship. On both Merapi and Kaitake, these elongated basins may further highlight the dynamics of basin  
438 competition on radial structures – through drainage divide migration and areal loss (likely influenced by edifice-  
439 scale sector collapses or regrowth events; Gertisser et al., 2023), less-erosive drainages become passive players to  
440 more dominant basins and adopt non-standard geometries, becoming narrow, chute-like basins on the mid- and  
441 upper-flanks.



442

443 **Figure 9** – Hack’s Law analysis of (a, c) Merapi and (b, d) Kaitake. **a-b**: Basin drainage area – length relationships. Black lines  
 444 represent Hack’s Law regressions. Colored circles correspond to the deviation from the regression trend (eq. 9), associated with  
 445 the color bars in c and d. Red-dashed line is imposed 1.0 km<sup>2</sup> channelization threshold, black dots are basins less than the  
 446 threshold and excluded from the regression. **c-d**: Semi-transparent hillshaded relief maps showing the deviation of each basin  
 447 from the best-fit power-law regression.

448 **4.5 How do radial drainages compare to other settings?**

449 Thus far, our discussion has focused on deriving a foundational understanding of how radial drainages on volcanic  
 450 edifices evolve and compete. However, we note similarities between our interpretation and those from previous  
 451 studies in other drainage settings. This leads to a simple question – is there a significant difference between radial  
 452 and dendritic drainage development and evolution?

453 Our results show that basin formation on volcanic edifices follows the development of rills and gullies within  
 454 badlands (Schumm, 1956). As radial drainages evolve and certain basins expand to become dominant features on the  
 455 edifice, less-dominant basins become passive and are pushed down-flank, often adhering to non-standard geometries  
 456 as imposed by their more-dominant neighbors (Habousha et al., 2023; Beeson and McCoy, 2022). The dynamics of

457 this basin competition and formation of passive basins are demonstrated by edifice basin spacing ratios. Summit  
458 basins on edifices have spacing ratios that appear time-independent and fit within the range of values observed in  
459 linear mountain ranges globally (Hovius, 1996) (Fig. 7), suggesting this ratio is set during the initial stages of basin  
460 formation – an attribute of basin evolution that has been shown to occur on linear fault blocks (Talling et al., 1997;  
461 Habousha et al., 2023). However, basins that are within a radial distance from the summit that is 30% of the  
462 edifice’s maximum radius do experience a temporally-decreasing spacing ratio and constant distance between  
463 outlets (Fig. 8), capturing the development of a basin topographic hierarchy along the edifice – a behavior not  
464 previously observed. Finally, our drainage divide analysis on volcanic edifices suggest that radial drainage basins  
465 evolve towards a stable basin configuration as topography matures towards a dynamic equilibrium, similar to  
466 regional landscape evolution globally (e.g., Perron and Royden, 2013; Willett et al., 2014).

467 This comparison suggests that drainage development and evolution on radial structures are largely similar to those  
468 occurring within linear mountain settings. However, some differences still occur, particularly in relation to basin  
469 geometries imposed by the larger-scale, radial primary landform. Dendritic drainages in linear mountain belts and  
470 fault blocks are characterized by their leaf-like geometries (e.g., Zernitz, 1932; Strahler, 1952; Talling et al., 1997),  
471 having a broad headwater region that decreases towards the outlet to a tapered point. Although radial drainages also  
472 have tapered outlets and basin widths increase upstream, these widths are hindered by the conical geometry of the  
473 primary landform and convergence of multiple basins towards the summit, leading to a tapered headwater as well as  
474 a tapered outlet. This geometric constraint is well-demonstrated by the drainages on Merapi (Fig. 9c), where summit  
475 basins are generally widest on the lower- or mid-flanks; however, this trend is not as obvious on Kaitake (Fig. 9d),  
476 where erosion has dissected the landform and weakened the conical influence of the edifice on basin geometries.  
477 Furthermore, as edifice drainages are limited to a conical landform, their evolution and configuration are constrained  
478 by a cumulative areal limit. As opposed to linear mountain ranges (where a morphologic change in one basin  
479 impacts its neighbors, which then impacts their neighbors as a cascading chain across the landscape), on volcanic  
480 edifices, a morphologic change in one basin (particularly a dominant basin) may directly impact the erosional state  
481 and morphology of most other basins on the landform due to the high number of basins that may share a divide with  
482 this basin. This areal effect on radial basin evolution may be further augmented by the higher diversity of underlying  
483 host rocks between edifice basins associated with magmatic and volcanic products (e.g., tephra deposits, lava flows,  
484 and intrusions) that is not as prevalent within linear mountain ranges.

485 Despite the differences in basin geometries and interactions discussed above, edifice-averaged morphometric values  
486 (e.g., Hack’s Law exponent, drainage density, mean basin hypsometry, mean basin slopes) are similar to those of  
487 other settings (Hack, 1957; Strahler, 1952; Horton, 1945). This suggests that although radial drainages experience  
488 phenomena that differ from those typically experienced in dendritic settings, drainage development, geometries, and  
489 competition largely follow those of dendritic patterns. As volcanic surfaces are easily datable and their ages can  
490 often vary by orders magnitude on a single edifice, volcanoes thus represent ideal locations for studying terrain  
491 evolution over varying temporal scales within a general framework.

492 **4.6 Basin morphology capturing volcanic processes**

493 In this study, we considered edifice morphologies using mean values over the entire edifice. However, our metrics  
494 also allow for the comparison of basin morphologies on a single edifice. Variations associated with these metrics  
495 would likely relate to spatially-localized attributes of aggradation, degradation, and climate, and would thus provide  
496 a quantitative method to disentangle these signals using topography. For example, edifice flanks that have been  
497 resurfaced by large volcanic deposits or destroyed by sector collapses should exhibit younger drainage networks  
498 according to the metrics explored here, and are expected to differ from other parts of the volcano. Furthermore,  
499 alterations to the erosional efficiency of a basin by tephra accumulation or lava flow emplacement should create  
500 spatial variability that can be quantified by similar analyses. These concepts should be tested over well-constrained  
501 cases and would be beneficial for both preliminary fieldwork and to approximate relative volcanic chronologies  
502 remotely. Our model for edifice degradation, radial drainage evolution, and divide stability thus provides a first step  
503 to deconvolving the various signals that relate to edifice morphology. This presents new avenues of exploration for  
504 the volcanology community to interrogate volcanic histories from topography, and for the geomorphic community to  
505 investigate surface evolution on landforms that often fall outside standard tectonic studies.

506 **5.0 Conclusion**

507 Volcanic edifices represent a class of primary landforms whose erosion remains relatively unexplored. We analyzed  
508 the degradational histories of stratovolcanoes using a set of metrics that have not previously been considered for  
509 radial drainage networks. We show that these metrics relate to the overall age of a volcano and propose a new  
510 general model for the temporal evolution of edifice drainage morphology. Divide stability analysis underscores the  
511 dynamic nature of basin evolution, and suggests that radial drainage networks initiate with nearly-uniform  
512 geometries and unstable configurations that evolve towards non-uniform basin geometries and more stable  
513 configurations to generate a basin topographic hierarchy on volcanoes. Finally, comparing basin geometries,  
514 configurations, and outlet spacing between basins that exist on volcanic edifices to those that exist on linear  
515 mountain ranges highlights similarities and differences between radial and dendritic drainage basins.

516 **6.0 Code availability**

517 DrainageVolc and MorVolc codes are available at [https://github.com/danjohara/Volc\\_Packages](https://github.com/danjohara/Volc_Packages).

518 **7.0 Data availability**

519 Collected edifice data is included in the supplement as both an Excel file and shapefile.

520 **8.0 Author contribution**

521 All authors provided editorial advice on the manuscript. DO'H wrote the DrainageVolc and updated MorVolc codes,  
522 conducted the morphology analyses, and wrote the manuscript. RMJvW assisted in data collection, determined  
523 edifice boundaries from topography, and tested DrainageVolc/MorVolc. LG and BC gave advice on drainage basin  
524 morphology and evolution, while PG, PL, and GK provided insight on volcanic edifice morphology, evolution, and  
525 general volcano ages. MK secured funds and coordinated the project, giving advice on the research direction,  
526 analyses, and interpretation.

527 **9.0 Competing interests**

528 The authors declare that they have no conflict of interest.

529 **10.0 Acknowledgement**

530 This research was funded through the EVoLvE project, Junior FWO project grant G029820N of the Fonds

531 Wetenschappelijke Onderzoek – Vlaanderen.

532 **11.0 References**

533 Becerril, L., Lara, L. E., and Astudillo, V. I.: The strong competition between growth and erosive processes on the  
534 Juan Fernández Archipelago (SE Pacific, Chile), *Geomorphology*, 373, 107513,  
535 <https://doi.org/10.1016/j.geomorph.2020.107513>, 2021.

536 Beeson, H. W. and McCoy: Disequilibrium river networks dissecting the western slope of the Sierra Nevada,  
537 California, USA, record significant late Cenozoic tilting and associated surface uplift, *Bull. Geol. Soc. Am.*, 134,  
538 2809–2853, <https://doi.org/10.1130/B36517.1>, 2022.

539 Biggs, J., Mothes, P., Ruiz, M., Amelung, F., Dixon, T. H., Baker, S., and Hong, S. H.: Stratovolcano growth by co-  
540 eruptive intrusion: The 2008 eruption of Tungurahua Ecuador, *Geophys. Res. Lett.*, 37,  
541 <https://doi.org/10.1029/2010GL044942>, 2010.

542 Bishop, P.: Drainage rearrangement by river capture, beheading and diversion, *Prog. Phys. Geogr.*, 19, 449–473,  
543 1995.

544 Bohnenstiehl, D. W. R., Howell, J. K., White, S. M., and Hey, R. N.: A modified basal outlining algorithm for  
545 identifying topographic highs from gridded elevation data, Part 1: Motivation and methods, *Comput. Geosci.*, 49,  
546 308–314, <https://doi.org/10.1016/j.cageo.2012.04.024>, 2012.

547 Braun, J.: A review of numerical modeling studies of passive margin escarpments leading to a new analytical  
548 expression for the rate of escarpment migration velocity, *Gondwana Res.*, 53, 209–224,  
549 <https://doi.org/10.1016/j.gr.2017.04.012>, 2018.

550 Castelltort, S. and Simpson, G.: River spacing and drainage network growth in widening mountain ranges, *Basin*  
551 *Res.*, 18, 267–276, <https://doi.org/10.1111/j.1365-2117.2006.00293.x>, 2006.

552 Castelltort, S., Simpson, G., and Darriulat, A.: Slope-control on the aspect ratio of river basins, *Terra Nov.*, 21,  
553 265–270, <https://doi.org/10.1111/j.1365-3121.2009.00880.x>, 2009.

554 Castelltort, S., Goren, L., Willett, S. D., Champagnac, J. D., Herman, F., and Braun, J.: River drainage patterns in  
555 the New Zealand Alps primarily controlled by plate tectonic strain, *Nat. Geosci.*, 5, 744–748,  
556 <https://doi.org/10.1038/ngeo1582>, 2012.

557 Castro, J. M., Cordonnier, B., Schipper, C. I., Tuffen, H., Baumann, T. S., and Feisel, Y.: Rapid laccolith intrusion  
558 driven by explosive volcanic eruption, *Nat. Commun.*, 7, 1–7, <https://doi.org/10.1038/ncomms13585>, 2016.

559 Civico, R., Ricci, T., Scarlato, P., Taddeucci, J., Andronico, D., Del Bello, E., D’Auria, L., Hernández, P. A., and  
560 Pérez, N. M.: High-resolution Digital Surface Model of the 2021 eruption deposit of Cumbre Vieja volcano, La  
561 Palma, Spain, *Sci. Data*, 9, 1–7, <https://doi.org/10.1038/s41597-022-01551-8>, 2022.

562 Cook, K. L., Turowski, J. M., and Hovius, N.: A demonstration of the importance of bedload transport for fluvial  
563 bedrock erosion and knickpoint propagation, *Earth Surf. Process. Landforms*, 38, 683–695,  
564 <https://doi.org/10.1002/esp.3313>, 2013.

565 Dibacto, S., Lahitte, P., Karátson, D., Hencz, M., Szakács, A., Biró, T., Kovács, I., and Veres, D.: Growth and  
566 erosion rates of the East Carpathians volcanoes constrained by numerical models: Tectonic and climatic  
567 implications, *Geomorphology*, 368, 107352, <https://doi.org/10.1016/j.geomorph.2020.107352>, 2020.

568 Duvall, A. R. and Tucker, G. E.: Dynamic Ridges and Valleys in a Strike-Slip Environment, *J. Geophys. Res. F*  
569 *Earth Surf.*, 120, 2016–2026, <https://doi.org/10.1002/2015JF003618>, 2015.

570 Euillades, L. D., Grosse, P., and Euillades, P. A.: NETVOLC: An algorithm for automatic delimitation of volcano  
571 edifice boundaries using DEMs, *Comput. Geosci.*, 56, 151–160, <https://doi.org/10.1016/j.cageo.2013.03.011>, 2013.

572 Farr, T. G., Rosen, P. A., Caro, E., Crippen, R., Duren, R., Hensley, S., Kobrick, M., Paller, M., Rodriguez, E.,  
573 Roth, L., Seal, D., Shaffer, S., Shimada, J., Umland, J., Werner, M., Oskin, M., Burbank, D., and Alsdorf, D.: The  
574 Shuttle Radar Topography Mission, *Rev. Geophys.*, 45, 1–43, 2007.

575 Ferrier, K. L., Huppert, K. L., and Perron, J. T.: Climatic control of bedrock river incision, *Nature*, 496, 206–209,  
576 <https://doi.org/10.1038/nature11982>, 2013.

577 Flint, J. J.: Stream gradient as a function of order, magnitude, and discharge, *Water Resour. Res.*, 10, 969–973,  
578 <https://doi.org/10.1029/WR010i005p00969>, 1974.

579 Forte, A. M. and Whipple, K. X.: Criteria and tools for determining drainage divide stability, *Earth Planet. Sci. Lett.*,  
580 493, 102–117, <https://doi.org/10.1016/j.epsl.2018.04.026>, 2018.

581 Fox, M., Goren, L., May, D. A., and Willett, S. D.: Inversion of fluvial channels for paleorock uplift rates in Taiwan,  
582 *J. Geophys. Res. Earth Surf.*, 119, 1853–1875, <https://doi.org/10.1002/2014JF003196>, 2014.

583 Gase, A. C., Brand, B. D., and Bradford, J. H.: Evidence of erosional self-channelization of pyroclastic density  
584 currents revealed by ground-penetrating radar imaging at Mount St. Helens, Washington (USA), *Geophys. Res.*  
585 *Lett.*, 44, 2220–2228, <https://doi.org/10.1002/2016GL072178>, 2017.

586 Gertisser, R., Troll, V. R., Walter, T. R., Nandaka, I. G. M. A., and Ratdomopurbo, A.: Merapi Volcano: Geology,  
587 Eruptive Activity, and Monitoring of a High-Risk Volcano, Springer Nature, 2023.

588 Gilbert, G. K.: The Convexity of Hilltops, *J. Geol.*, 17, 344–350, 1909.

589 Global Volcanism Program: Volcanoes of the World, v. 4.10.5 (27 Jan 2022), Smithsonian Inst., 2013.

590 Grosse, P., van Wyk de Vries, B., Petrinovic, I. A., Euillades, P. A., and Alvarado, G. E.: Morphometry and  
591 evolution of arc volcanoes, *Geology*, 37, 651–654, <https://doi.org/10.1130/G25734A.1>, 2009.

592 Grosse, P., van Wyk de Vries, B., Euillades, P. A., Kervyn, M., and Petrinovic, I. A.: Systematic morphometric  
593 characterization of volcanic edifices using digital elevation models, *Geomorphology*, 136, 114–131,  
594 <https://doi.org/10.1016/j.geomorph.2011.06.001>, 2012.

595 Haapala, J. M., Escobar Wolf, R., Vallance, J. W., Rose, W. I., Griswold, J. P., Schiling, S. P., Ewert, J. W., and  
596 Mota, M.: Volcanic Hazards at Atitlán Volcano, Guatemala, Open-File Rep., 2005.

597 Habousha, K., Goren, L., Nativ, R., and Gruber, C.: Plan-Form Evolution of Drainage Basins in Response to  
598 Tectonic Changes: Insights From Experimental and Numerical Landscapes, *J. Geophys. Res. Earth Surf.*, 128, 1–24,  
599 <https://doi.org/10.1029/2022jf006876>, 2023.

600 Hack, J. T.: Studies of longitudinal stream profiles in Virginia and Maryland, USGS Prof. Pap. 249, 97, 1957.

601 Hamawi, M., Goren, L., Mushkin, A., and Levi, T.: Rectangular drainage pattern evolution controlled by pipe cave  
602 collapse along clastic dikes, the Dead Sea Basin, Israel, *Earth Surf. Process. Landforms*, 47, 936–954,  
603 <https://doi.org/10.1002/esp.5295>, 2022.

604 Han, J., Gasparini, N. M., and Johnson, J. P. L.: Measuring the imprint of orographic rainfall gradients on the  
605 morphology of steady-state numerical fluvial landscapes, *Earth Surf. Process. Landforms*, 40, 1334–1350,  
606 <https://doi.org/10.1002/esp.3723>, 2015.

607 Hasbargen, L. E. and Paola, C.: Landscape instability in an experimental drainage basin, *Geology*, 28, 1067–1070,  
608 [https://doi.org/10.1130/0091-7613\(2000\)28<1067:LIIAED>2.0.CO;2](https://doi.org/10.1130/0091-7613(2000)28<1067:LIIAED>2.0.CO;2), 2000.

609 Hayes, S. K., Montgomery, D. R., and Newhall, C. G.: Fluvial sediment transport and deposition following the 1991  
610 eruption of Mount Pinatubo, *Geomorphology*, 45, 211–224, [https://doi.org/10.1016/S0169-555X\(01\)00155-6](https://doi.org/10.1016/S0169-555X(01)00155-6), 2002.

611 Horton, R. E.: Erosional development of streams and their drainage basins; hydrological approach to quantitative  
612 morphology, *Geol. Soc. Am. Bull.*, 56, 275–370, <https://doi.org/10.1130/0016->

613 7606(1945)56[275:EDOSAT]2.0.CO;2, 1945.

614 Hovius, N.: Regular spacing of drainage outlets from linear mountain belts, *Basin Res.*, 8, 29–44,  
615 <https://doi.org/10.1111/j.1365-2117.1996.tb00113.x>, 1996.

616 Howard, A. D.: Drainage Analysis in Geologic Interpretation: A Summation, *Am. Assoc. Pet. Geol. Bull.*, 51,  
617 <https://doi.org/10.1306/5d25c26d-16c1-11d7-8645000102c1865d>, 1967.

618 Jefferson, A., Grant, G. E., Lewis, S. L., and Lancaster, S. T.: Coevolution of hydrology and topography on a basalt  
619 landscape in the Oregon Cascade Range, USA, *Earth Surf. Process. Landforms*, 35, 803–816,  
620 <https://doi.org/10.1002/esp.1976>, 2010.

621 Karátson, D., Thouret, J. C., Moriya, I., and Lomoschitz, A.: Erosion calderas: Origins, processes, structural and  
622 climatic control, *Bull. Volcanol.*, 61, 174–193, <https://doi.org/10.1007/s004450050270>, 1999.

623 Karátson, D., Telbisz, T., and Wörner, G.: Erosion rates and erosion patterns of Neogene to Quaternary  
624 stratovolcanoes in the Western Cordillera of the Central Andes: An SRTM DEM based analysis, *Geomorphology*,  
625 139–140, 122–135, <https://doi.org/10.1016/j.geomorph.2011.10.010>, 2012.

626 Kerr, R. C.: Thermal erosion by laminar lava flows, *J. Geophys. Res. B Solid Earth*, 106, 453–465,  
627 <https://doi.org/10.1029/2001JB000227>, 2001.

628 Kirby, E. and Whipple, K. X.: Expression of active tectonics in erosional landscapes, *J. Struct. Geol.*, 44, 54–75,  
629 <https://doi.org/10.1016/j.jsg.2012.07.009>, 2012.

630 Kirby, E., Whipple, K. X., Tang, W., and Chen, Z.: Distribution of active rock uplift along the eastern margin of the  
631 Tibetan Plateau: Inferences from bedrock channel longitudinal profiles, *J. Geophys. Res. Solid Earth*, 108,  
632 <https://doi.org/10.1029/2001JB000861>, 2003.

633 Lahitte, P., Samper, A., and Quidelleur, X.: DEM-based reconstruction of southern Basse-Terre volcanoes  
634 (Guadeloupe archipelago, FWI): Contribution to the Lesser Antilles Arc construction rates and magma production,  
635 *Geomorphology*, 136, 148–164, <https://doi.org/10.1016/j.geomorph.2011.04.008>, 2012.

636 Locke, C. A. and Cassidy, J.: Egmont Volcano, New Zealand: Three-dimensional structure and its implications for  
637 evolution, *J. Volcanol. Geotherm. Res.*, 76, 149–161, [https://doi.org/10.1016/S0377-0273\(96\)00074-1](https://doi.org/10.1016/S0377-0273(96)00074-1), 1997.

638 Lohse, K. A. and Dietrich, W. E.: Contrasting effects of soil development on hydrological properties and flow paths,  
639 *Water Resour. Res.*, 41, 1–17, <https://doi.org/10.1029/2004WR003403>, 2005.

640 Major, J. J., Mosbrucker, A. R., and Spicer, K. R.: Sediment erosion and delivery from Toutle River basin after the  
641 1980 eruption of Mount St. Helens: A 30-year perspective, *Ecol. Responses Mt. St. Helens Revisit. 35 years after*  
642 *1980 Erupt.*, 19–44, [https://doi.org/10.1007/978-1-4939-7451-1\\_2](https://doi.org/10.1007/978-1-4939-7451-1_2), 2018.

643 McBirney, A. R., Serva, L., Guerra, M., and Connor, C. B.: Volcanic and seismic hazards at a proposed nuclear  
644 power site in central Java, *J. Volcanol. Geotherm. Res.*, 126, 11–30, [https://doi.org/10.1016/S0377-0273\(03\)00114-](https://doi.org/10.1016/S0377-0273(03)00114-8)  
645 8, 2003.

646 Mejía, A. I. and Niemann, J. D.: Identification and characterization of dendritic, parallel, pinnate, rectangular, and  
647 trellis networks based on deviations from planform self-similarity, *J. Geophys. Res. Earth Surf.*, 113, 1–21,  
648 <https://doi.org/10.1029/2007JF000781>, 2008.

649 Montgomery, D. R. and Dietrich, W. E.: Landscape Dissection and Drainage Area-Slope Threshold, in: *Process*  
650 *Models and Theoretical Geomorphology*, 1994.

651 Mudd, S. M. and Furbish, D. J.: Responses of soil-mantled hillslopes to transient channel incision rates, *J. Geophys.*  
652 *Res. Earth Surf.*, 112, 1–12, <https://doi.org/10.1029/2006JF000516>, 2007.

653 Mueller, J. E.: Re-evaluation of the relationship of master streams and drainage basins, *Bull. Geol. Soc. Am.*, 83,  
654 3471–3474, [https://doi.org/10.1130/0016-7606\(1972\)83\[3471:ROTRROM\]2.0.CO;2](https://doi.org/10.1130/0016-7606(1972)83[3471:ROTRROM]2.0.CO;2), 1972.

655 Mulyaningsih, S. and Shaban, G.: Geochemistry of basaltic Merbabu volcanic rocks, Central Java, Indonesia,

- 656 Indones. J. Geosci., 7, 161–178, <https://doi.org/10.17014/ijog.7.2.161-178>, 2020.
- 657 O’Hara, D. and Karlstrom, L.: The arc-scale spatial distribution of volcano erosion implies coupled magmatism and  
658 regional climate in the Cascades arc, United States, *Front. Earth Sci.*, 11, 1–15,  
659 <https://doi.org/10.3389/feart.2023.1150760>, 2023.
- 660 O’Hara, D., Karlstrom, L., and Roering, J. J.: Distributed landscape response to localized uplift and the fragility of  
661 steady states, *Earth Planet. Sci. Lett.*, 506, 243–254, <https://doi.org/10.1016/j.epsl.2018.11.006>, 2019.
- 662 O’Hara, D., Karlstrom, L., and Ramsey, D. W.: Time-evolving surface and subsurface signatures of Quaternary  
663 volcanism in the Cascades arc, *Geology*, 49, e526, <https://doi.org/10.1130/g47706.1>, 2020.
- 664 Ollier, C.: *Volcanoes*, edited by: Blackwell, B., Oxford., 288 pp., 1988.
- 665 Perron, J. T. and Royden, L.: An integral approach to bedrock river profile analysis, *Earth Surf. Process. Landforms*,  
666 38, 570–576, <https://doi.org/10.1002/esp.3302>, 2013.
- 667 Pierson, T. C. and Major, J. J.: Hydrogeomorphic effects of explosive volcanic eruptions on drainage basins, *Annu.*  
668 *Rev. Earth Planet. Sci.*, 42, 469–507, <https://doi.org/10.1146/annurev-earth-060313-054913>, 2014.
- 669 Prince, P. S. and Spotila, J. A.: Evidence of transient topographic disequilibrium in a landward passive margin river  
670 system: Knickpoints and paleo-landscapes of the New River basin, southern Appalachians, *Earth Surf. Process.*  
671 *Landforms*, 38, 1685–1699, <https://doi.org/10.1002/esp.3406>, 2013.
- 672 Ricci, J., Lahitte, P., and Quidelleur, X.: Construction and destruction rates of volcanoes within tropical  
673 environment: Examples from the Basse-Terre Island (Guadeloupe, Lesser Antilles), *Geomorphology*, 228, 597–607,  
674 <https://doi.org/10.1016/j.geomorph.2014.10.002>, 2015.
- 675 Scherler, D. and Schwanghart, W.: Drainage divide networks - Part 1: Identification and ordering in digital elevation  
676 models, *Earth Surf. Dyn.*, 8, 245–259, <https://doi.org/10.5194/esurf-8-245-2020>, 2020.
- 677 Schumm, S. A.: Evolution of drainage systems and slopes in badlands at Perth Amboy, New Jersey, *Bull. Geol. Soc.*  
678 *Am.*, 67, 597–646, [https://doi.org/10.1130/0016-7606\(1956\)67\[597:EODSAS\]2.0.CO;2](https://doi.org/10.1130/0016-7606(1956)67[597:EODSAS]2.0.CO;2), 1956.
- 679 Schwanghart, W. and Scherler, D.: Short Communication: TopoToolbox 2 - MATLAB-based software for  
680 topographic analysis and modeling in Earth surface sciences, *Earth Surf. Dyn.*, 2, 1–7, <https://doi.org/10.5194/esurf-2-1-2014>, 2014.
- 682 Shea, T. and van Wyk de Vries, B.: Structural analysis and analogue modeling of the kinematics and dynamics of  
683 rockslide avalanches, *Geosphere*, 4, 657–686, <https://doi.org/10.1130/GES00131.1>, 2008.
- 684 Sklar, L. S. and Dietrich, W. E.: Sediment and rock strength controls on river incision into bedrock, *Geology*, 29,  
685 1087–1090, [https://doi.org/10.1130/0091-7613\(2001\)029<1087:SARSCO>2.0.CO;2](https://doi.org/10.1130/0091-7613(2001)029<1087:SARSCO>2.0.CO;2), 2001.
- 686 Strahler, A. N.: Hypsometric (area-altitude) analysis of erosional topography, *Bull. Geol. Soc. Am.*, 63, 1117–1142,  
687 <https://doi.org/10.1128/AAC.03728-14>, 1952.
- 688 Sweeney, K. E. and Roering, J. J.: Rapid fluvial incision of a late Holocene lava flow: Insights from LiDAR, alluvial  
689 stratigraphy, and numerical modeling, *Bull. Geol. Soc. Am.*, 129, 500–512, <https://doi.org/10.1130/B31537.1>, 2017.
- 690 Talling, P. J., Stewart, M. D., Stark, C. P., Gupta, S., and Vincent, S. J.: Regular spacing of drainage outlets from  
691 linear fault blocks, *Basin Res.*, 9, 275–302, <https://doi.org/10.1046/j.1365-2117.1997.00048.x>, 1997.
- 692 Thouret, J. C., Oehler, J. F., Gupta, A., Solikhin, A., and Procter, J. N.: Erosion and aggradation on persistently  
693 active volcanoes—a case study from Semeru Volcano, Indonesia, *Bull. Volcanol.*, 76,  
694 <https://doi.org/10.1007/s00445-014-0857-z>, 2014.
- 695 Ui, T. and Glicken, H.: Internal structural variations in a debris-avalanche deposit from ancestral Mount Shasta,  
696 California, USA, *Bull. Volcanol.*, 48, 189–194, <https://doi.org/10.1007/BF01087673>, 1986.
- 697 van Wees, R. M. J., Tournigand, P.-Y., O’Hara, D., Grosse, P., Kereszturi, G., Campforts, B., Lahitte, P., and  
698 Kervyn, M.: The role of erosion in the morphometry of composite volcanoes, in: EGU General Assembly



699 Conference Abstracts, EGU21-14500, 2021.

700 van Wees, R. M. J., O'Hara, D., Kereszturi, G., Grosse, P., Lahitte, P., Tourniganda, P.-Y., and Kervyn, M.:  
701 Towards more consistent volcano morphometry datasets: Assessing boundary delineation and DEM impact on  
702 geometric and drainage parameters, *Geomorphology*, in review.

703 Wells, S. G., Dohrenwend, J. C., McFadden, L. D., Turrin, B. D., and Mahrer, K. D.: Late Cenozoic landscape  
704 evolution on lava flow surfaces of the Cima volcanic field, Mojave Desert, California., *Geol. Soc. Am. Bull.*, 96,  
705 1518–1529, [https://doi.org/10.1130/0016-7606\(1985\)96<1518:LCLEOL>2.0.CO;2](https://doi.org/10.1130/0016-7606(1985)96<1518:LCLEOL>2.0.CO;2), 1985.

706 Whipple, K. X., DiBiase, R. A., Ouimet, W. B., and Forte, A. M.: Preservation or piracy: Diagnosing low-relief,  
707 high-elevation surface formation mechanisms, *Geology*, 45, 91–94, <https://doi.org/10.1130/G32501Y.1>, 2016.

708 Wicks, C. W., Dzurisin, D., Ingebritsen, S., Thatcher, W., Lu, Z., and Iverson, J.: Magmatic activity beneath the  
709 quiescent Three Sisters volcanic center, central Oregon Cascade Range, USA, *Geophys. Res. Lett.*, 29, 26-1-26–4,  
710 <https://doi.org/10.1029/2001GL014205>, 2002.

711 Willett, S. D., Slingerland, R., and Hovius, N.: Uplift, shortening, and steady state topography in active mountain  
712 belts, *Am. J. Sci.*, 301, 455–485, <https://doi.org/10.2475/ajs.301.4-5.455>, 2001.

713 Willett, S. D., McCoy, S. W., Perron, T. J., Goren, L., and Chen, C. Y.: Dynamic reorganization of River Basins,  
714 *Science (80- )*, 343, <https://doi.org/10.1126/science.1248765>, 2014.

715 Yang, R., Willett, S. D., and Goren, L.: In situ low-relief landscape formation as a result of river network disruption,  
716 *Nature*, 520, 526–529, <https://doi.org/10.1038/nature14354>, 2015.

717 Zernitz, E. R.: Drainage Patterns and Their Significance, *J. Geol.*, 40, 498–521, <https://doi.org/10.1086/623976>,  
718 1932.

719